Experimental investigation of crack propagation and crack branching in lightly reinforced concrete beams using Digital Image Correlation

Experimental investigation of crack propagation and crack branching in lightly reinforced concrete beams using Digital Image Correlation

Tahreer M. Fayyad and Janet M. Lees

Abstract

Relatively few fracture-oriented experimental studies have been conducted on concrete that is reinforced. An experimental investigation was therefore undertaken to explore the cracking process in lightly reinforced concrete (RC) beams and to observe the details of the localised fracture process zone development. More specifically, the aims were to investigate the relationships between beam height (120 mm, 220 mm and 320 mm), steel reinforcement ratio (0.1%-0.5%), ductility and the onset of crack branching. RC beams were tested in three-point bending and experimental surface strains and crack openings were inferred using digital image correlation (DIC). It was found that the presence of the reinforcement prevented premature fracture and led to crack branching where a single crack bifurcated in the region of the compression zone. In the larger beams the branching developed at a lower relative height and a greater reinforcement ratio led to a shallower branching angle. These observations were associated with ductility measures for lightly reinforced concrete beams.

Key words

RC crack propagation, crack branching, bifurcation, ductility, size effect

1. Introduction

Concrete is a quasi-brittle material that has a relatively weak tensile strength when compared with its compressive strength. It is therefore susceptible to cracking. Over the past decades the mechanics of concrete cracking have been investigated using different approaches such as finite element analyses, linear fracture mechanics (LFM) and non-linear fracture mechanics (NLFM), to develop models to simulate concrete cracking [1–8]. The cracking process in concrete is complex because the crack itself is a partially damaged zone with some capability for stress-transfer in the fracture process zone (FPZ). The FPZ acts as a transition zone between the discontinuous open crack and the continuous intact material beyond the crack. Although there is some debate about what constitutes a FPZ, and the size of the FPZ, there is a general agreement that it exists in concrete [9]. A realistic description of the FPZ is essential in order to understand damage mechanisms and to predict and optimize the behaviour of concrete structures. The FPZ is also important in determining a characteristic length of the microstructure that reflects size effects [10,11]. Theoretical studies have been conducted to understand the nature of the FPZ in concrete. Wecharatana and Shah [12] developed a theoretical model to predict the FPZ length where it was found that the length of the FPZ remains constant during

slow crack growth. However, theoretical calculations of the length of the FPZ are very sensitive to the value of the critical crack mouth opening displacement (CMOD) [12].

Various experimental techniques such as optical interferometry and imaging analysis techniques have also been adapted to investigate the extent of the FPZ. This is a challenging undertaking due to the existence of high localised stresses and strains in the FPZ which cannot be measured using standard gauges. An early attempt to investigate the strain field around the FPZ was undertaken by Cedolin et al. [13] who used optical interferometry to map the FPZ with contour lines of equal deformation. A more recent development is the use of digital image correlation (DIC) to measure the width of the FPZ in unreinforced concrete [10].

In reinforced concrete, the fracture process is further complicated by the presence of the reinforcement that affects the crack development and propagation. The cracking process is associated with diverse phenomena such as the formation of cracks, crack propagation, the existence of micro-cracks, interactions between the reinforcement and concrete, and the concrete microstructure e.g. cement and aggregate [2]. In addition, numerous factors can influence the cracking process and reinforcement crack bridging including the concrete compressive strength, the type, the properties and the ratio of the longitudinal reinforcement, the bond between the reinforcement and the concrete, and the geometrical properties and the size of the beam. These factors can be inter-related and inter-dependant. Furthermore, the cracking process in reinforced concrete (RC) may involve several macro-cracks propagating at the same time leading to different failure modes. Internal reinforcement bridges a crack and improves the fracture toughness by providing a stitching action that prevents the crack faces from opening and controls the crack growth by increasing the energy demand for crack advancement [14]. The fracture energy is closely related to the FPZ size and this implies that the existence of a FPZ may be the intrinsic cause for size effects. In concrete the FPZ covers a narrow crack band and only the region along the crack path is affected by cracking [15–17]. However, in reinforced concrete the nature of the FPZ remains unclear. Most theoretical studies incorporate the reinforcement according to the principle of superposition by considering concrete fracture and adding the effect of the reinforcement as a closing force [4,7,18–20]. Although the fracture properties of reinforced concrete at the structural scale have been studied, there is a need for further detailed investigations to better understand the nature of the fracture process.

A survey of literature in this field shows that relatively few experimental studies have investigated the fracture process in reinforced concrete as opposed to unreinforced concrete. Digital image correlation (DIC) has been used to evaluate the displacement and strain fields in bending tests on RC beams [21] where the focus was to test the performance of DIC and demonstrate its potential for investigating fracture properties. Skarzynski and Tejchman [16] tested small RC beams with a height of 80 mm and length 320 mm (effective length 240 mm) with a reinforcement ratio of 1.5%. It was found that the

localised zones are always created prior to the attainment of the peak load and the lengths of the fracture zones in RC beams (0.8 of the beam height) are higher than those in unreinforced concrete beams (0.6 of the beam height). Alam et al. [22] used Acoustic Emission (AE) to study microcracking in RC beams. It was found that as the beam size increases, the fracture process changes from tensile-microcracking-macrocracking to shear-compression macrocracking. Digital image correlation has also been used to study the cracking in reinforced concrete beams failing in shear [23] and it was found that the observed size effect was in agreement with Bazant's size effect [24].

Ductility is implicitly linked to the energy dissipation. Ductility in RC structures can be defined as the ability of a material to provide sufficient inelastic deformation beyond yielding and prior to failure. The importance of ductility in steel RC is that the steel consumes applied energy in irreversible inelastic displacement after yielding. This means that what happens during crack growth (or arrest) would affect the ductility and the structural behaviour. There is debate about how best to quantify ductility because deformation can be translated into different measures such as curvature, rotation and displacement [25,26]. A displacement-based ductility factor can be defined as $\mu = \frac{\Delta_{max}}{\Delta_y}$, where Δ_{max} is the maximum displacement and Δ_y is the displacement at yielding based on the load-deflection behaviour. However, the maximum displacement can be open to different interpretations especially when measured in a displacement-controlled test. One option is to define the maximum displacement as the maximum displacement at the maximum attained load, although a small reduction in the load after the peak load can be taken into account [27]. In a cracked beam, ductility can also be defined using fracture mechanics formulations as being associated with the propagation of a crack in a stable manner [28]. Stable behaviour is associated with fracture development with increasing load whereas unstable behaviour is associated with crack propagation with decreasing load.

Energy consuming mechanisms can also take the form of crack branching. Crack branching is a material toughening mechanism. This mainly occurs when some of the micro-cracks ahead of the crack tip are arrested, thus more energy is required for crack propagation and this can lead to crack branching. In reinforced concrete, the presence of the reinforcement provides bridging to the crack and hence a confining effect to the crack path. This may increase the possibility of crack branching where crack branching and the redistribution of stresses that take place during the failure process contribute to a more ductile failure behaviour [29]. Hence, if the amount of reinforcement affects the crack propagation process and the failure mode, it can be a source of a 'size effect' in RC beams.

The research will capitalise on recent developments in image processing techniques and high resolution digital cameras to provide advanced tools to measure fracture properties and insight into the FPZ in reinforced concrete. DIC provides a non-destructive and non-contact method for measuring the surface deformation of an object subjected to forces where images are compared at

different loading stages [10,15,17,21,23,30–34]. One of the main advantages of using this technique to analyse the cracking process is the possibility of obtaining a complete reconstruction of the crack geometry.

2. Research significance

Understanding cracking in reinforced concrete is important for the strength assessment and renovation of existing structures. Relatively few fracture-oriented experimental studies have been conducted on concrete with internal steel reinforcement. Knowledge of concrete fracture processes can help identify suitable analytical approaches that capture the details of the crack process. This study presents an experimental investigation of RC beams subjected to three point bending. A particular focus is the localised zone around the crack and the crack branching phenomena. Crack branching is a toughening mechanism in quasi-brittle materials and can be a source of size effects. Yet it has received little or no attention when studying the fracture of RC beams. In reinforced concrete, the confinement provided by the reinforcement to the crack path increases the possibility of crack branching. The crack branching that takes places during the failure process makes the failure behaviour more ductile. The aim of this research is to experimentally determine the relationship between size, reinforcement ratio and ductility through an investigation of crack branching in RC. The digital image correlation technique is used as an advanced tool to measure fracture and monitor the crack profile. Although more experiments are required to generalize the results, the research acts as a foundation to describe the flexural behaviour of lightly reinforced concrete beams and for further investigations of RC fracture processes.

3. Experimental Investigation

To investigate mode I fracture, flexural beam specimens were designed. The mode I results can also provide insight for theoretical studies of shear since it has been found that inclined crack propagation in reinforced concrete beams can be modelled as mode I fracture [7,35–37].

3.1. Experimental design

The experimental work was undertaken to study the cracking process and to investigate the nature of fracture in RC beams. In reinforced concrete, the reinforcement provides a confinement to the crack path which can be a source of size effect and may lead to other toughening mechanisms such as crack branching. Hence, different reinforcement ratios were used in the experimental program to study the effect of the reinforcement on beam ductility and different beam heights were considered to investigate the size effects. As the intention was for the RC beams to fail in flexure, for each beam size and a given concrete strength, the reinforcement ratios were selected such that the flexural capacity was less than the shear capacity. Flexural failures are common in lightly reinforced concrete beams or beams with shear reinforcement. However, more heavily reinforced concrete beams without

sufficient transverse steel will be predisposed to shear failures. Since the focus was to promote flexural failures, both the ACI standard (ACI 318M-11) [38] and the European Standard (EC2) [39] were used to predict the minimum shear capacity of the designed specimens. The predicted shear capacity according to the ACI approach does not depend on the longitudinal reinforcement ratio whereas the EC2 expression takes the longitudinal reinforcement ratio into consideration. The lower of the two predictions was used to ensure that the design flexural capacity was more critical. The flexural capacity was calculated based on an ultimate limit state analysis using an equivalent rectangular stress block.

3.2. Experimental program

A total of sixteen unreinforced and reinforced concrete beams were tested in three point bending. The flexural crack propagation was tracked using DIC. The unreinforced and reinforced concrete beams did not have shear links (Figure 1). The first series included nine beams with different longitudinal reinforcement ratios (0%, 0.15%, 0.2%, 0.3% and 0.5%) cast from a mix with a design concrete cube compressive strength of 45MPa. Three different beam sizes were considered but a constant clear span to effective height ratio was maintained (heights of 120 mm, 220 mm and 320 mm and lengths of 840 mm, 1700 mm and 2500 mm respectively). The second series included seven unreinforced and reinforced concrete beams cast from a mix with a target compressive strength of 30MPa. Two beam sizes (heights of 120 and 220 mm and lengths of 840 mm and 1700 mm respectively) and different reinforcement ratios (0%, 0.15%, 0.3%, 0.4% and 0.5%) were used. All the test beams had a width of 100mm and a concrete cover of 18mm. In Table 1 each beam has been identified using the following notation: a letter M followed by a number (showing the concrete mix strength), a letter D followed by a number (showing the effective depth), and then the reinforcement ratio as a %. The longitudinal steel consisted of deformed steel bars with average yield strength of 548MPa for bars with a 6mm nominal diameter and 537MPa for the 8mm diameter bars. The concrete mix (Table 2) used rapid hardening cement and aggregate with the particle size distribution shown in Figure 2. For monitoring the strain in the reinforcement bars, prior to casting, strain gauges were installed and protected by silicon on the surface of the reinforcement. For the small beams the gauges were located at mid span. For the medium and large beams the gauges were offset by 100mm from the mid span. A crack inducer was located at mid-span. Insulation foam was used to form the crack inducer where the foam was cut into pieces with a width of 6 mm and depths of 30, 40 and 50mm for the small, medium and large beams respectively. The foam was inserted vertically in the middle of the formwork prior to casting.

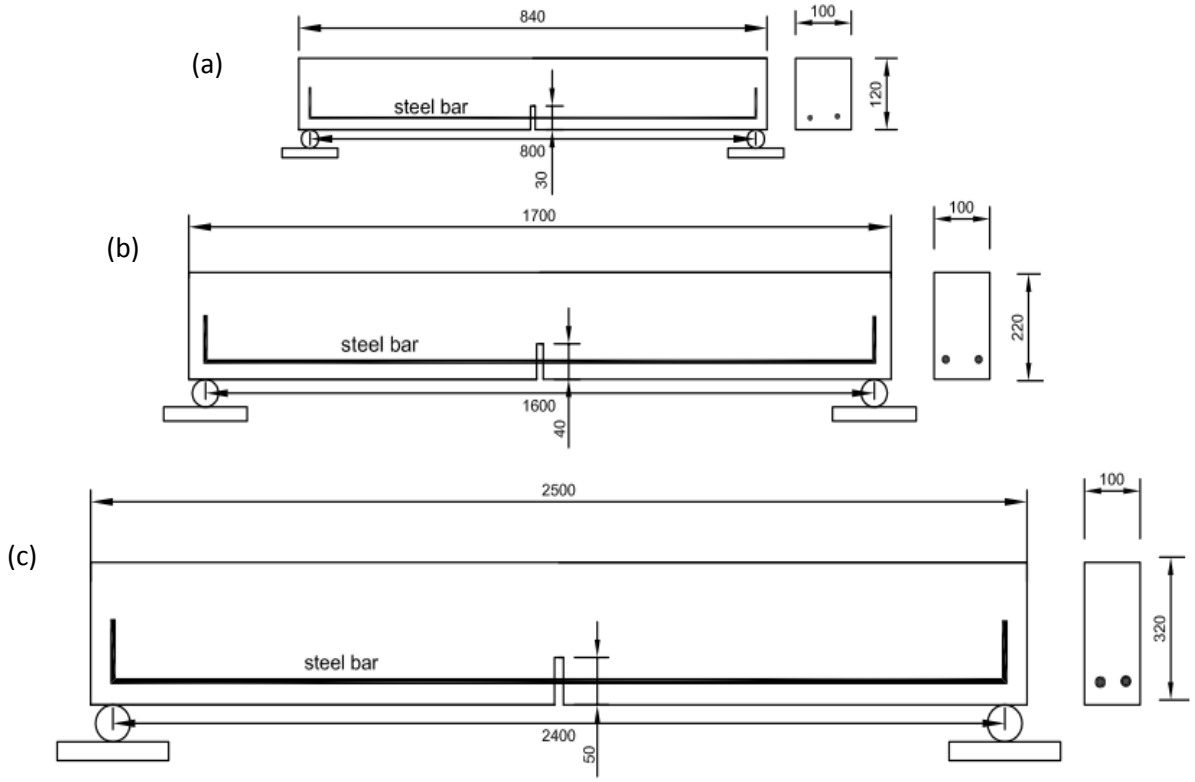

Figure 1 Test specimen layout (dimensions in mm); (a) small beam, (b)medium beam, (c) large beam

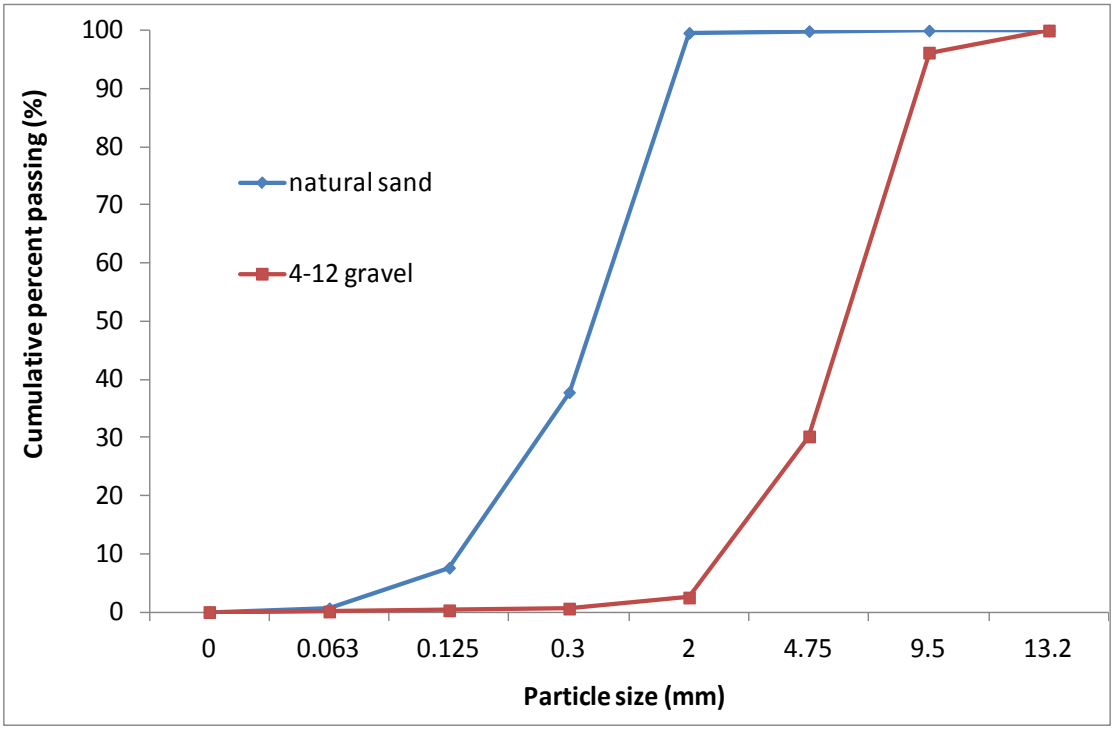

Figure 2 Aggregate particle size distribution

Table 1 Details of test specimens

Concrete cube compressive strength (MPa)	Beam dimensions Width×Height×Length (mm) × (mm) × (mm)	Reinforcement (ratio)	Notation
M_1= 45	100×320×2500	2T6 (0.2%)	M45,D300,0.2
		3T6 (0.3%)	M45,D300,0.3
		Unreinforced (0%)	M45,D300,0
	100×220×1700	1T6 (0.15%)	M45,D200,0.15
		2T6 (0.3%)	M45,D200,0.3
		Unreinforced (0%)	M45,D200,0
	100×120×840	1T6 (0.3%)	M45,D100,0.3
		1T8 (0.5%)	M45,D100,0.5
		Unreinforced (0%)	M45,D100,0
M_2 = 30	100×220×1700	1T6 (0.15%)	M30,D200,0.15
		2T6 (0.3%)	M30,D200,0.3
		3T6 (0.4%)	M30,D200,0.4
		Unreinforced (0%)	M30,D200,0
	100×120×840	1T6 (0.3%)	M30,D100,0.3
		1T8 (0.5%)	M30,D100,0.5
		Unreinforced (0%)	M30,D100,0

Table 2 Concrete mixes

Material	Mass required per m^3 (kg)	
	Mix (a) (30MPa)	Mix (b) (45MPa)
Cement	325	482
Water	205	205
Sand	774	684
aggregate	1025	985

3.3. DIC experimental setup and specimen preparation

In a DIC analysis, a reference image of the target area is split into small patches. These patches are tracked from one image to the next. It is then possible to measure the full field deformation of a selected area. To accurately track the patches, each patch should have characteristics that can be

distinguished from other patches. In the current work, the intensity of the pixels is used as the identification parameter. Pan et al. [40] found that the surface texture has a significant influence on the tracking results. Although there is no clear definition of what texture means, in DIC "a poor texture" would be associated with many patches having similar features whereas multi-coloured images are good examples of "a good texture". To get a random colour intensity distribution and a fairly good variation in the surface texture, the area of interest in the test specimens was sprayed using six different colours; red, green, blue, yellow, white and black to give each patch a unique speckle pattern. This uniqueness is essential in the matching process to decrease the measurement bias and noise [41]. Figure 3 shows a magnified region in the sprayed area and Figure 4 shows the intensity histogram for the three channels red, green and blue. The figure shows a fairly wide range of intensity distributions with peaks at around 50, 100 and 150. A digital single lens reflex (DSLR) camera with a 35 megapixel CMOS sensor was used to record images of the test specimens under loading. The camera was mounted on a tripod with its axis perpendicular to the area of interest. The camera had a focal length of 24-120 mm. Out-of-plane movement was not expected to be an issue but nevertheless, to minimize the effect of any out-of-plane movement, the camera was fixed a distance of 1000mm away from the specimen surface as recommended in [42]. The camera was directed towards the middle of the beam where flexural cracks were expected to develop. The obtained spatial resolution differs according to the region of interest which in turn differs according to the beam dimensions. For this setup, one pixel in the image represents about 30μm on the surface of the large beams. For some beams, a second DSLR camera was used either to give a greater resolution in the FPZ or to record the crack propagation on the other side of the beam. External lighting was directed toward the region of interest to enhance the image quality. During the test, the images were shot continuously every 10 seconds.

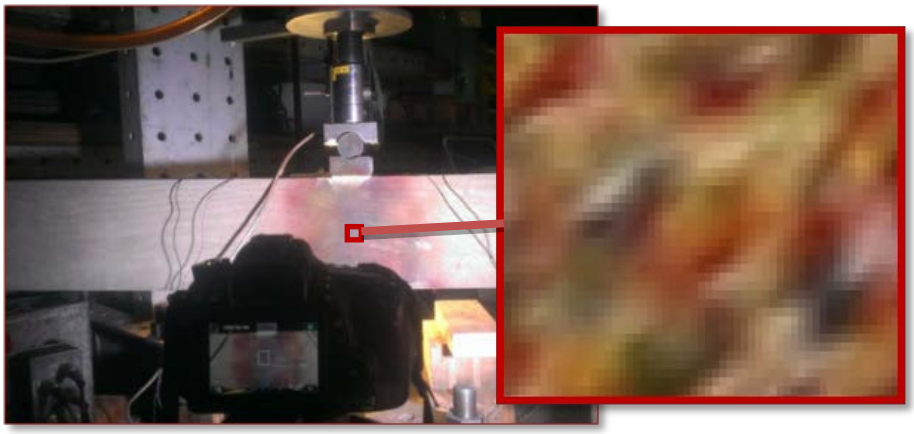

Figure 3 Test specimen surface texture

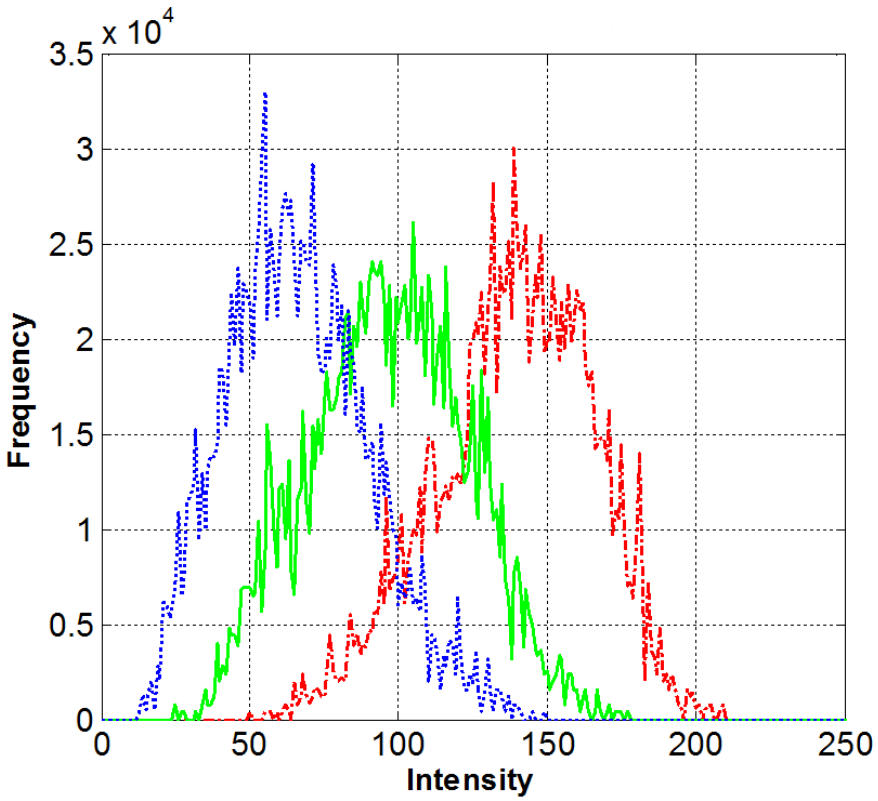

Figure 4 Intensity distribution over the surface of test beam

3.4. Testing

Each beam was tested to failure under three-point loading (Figure 5). The beams with a height of 120mm were tested in a servo-controlled Instron machine where the beams were supported on a wide flange steel beam (Figure 6). This meant that the beams could be positioned in the machine at an angle such that the side faces were visible. A bespoke rig was constructed to test the medium and large beams (Figure 7). In both setups, the end supports were two plates with a roller which allowed rotation and horizontal displacement. With the exception of the Instron loading plate that had a width of 20 mm, the widths of all the bearing pads were 75 mm. A C-clip was attached below the central notch of each beam to measure the crack mouth opening.

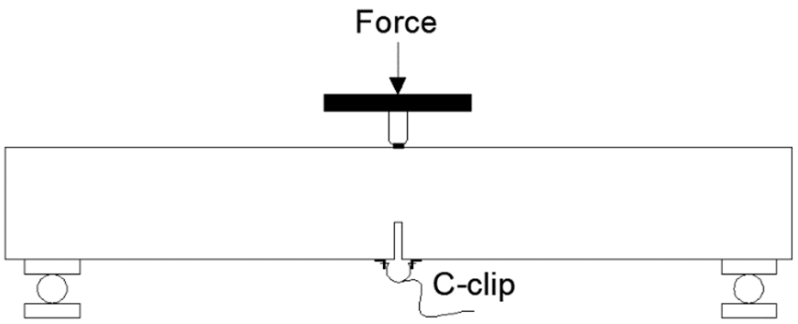

Figure 5 Test layout

In order to obtain stable loading conditions, all the tests were performed under displacement control. Consequently, the load was applied as a function of the mid span deflection. This allowed a gradual increase in the mid span deflection and crack mouth opening, as well as a steady decrease of the load in the post-peak regime. In the large beam test rig, the loading jack was connected to a hydraulic servo controlled machine to achieve a constant deflection rate; however, there was a certain delay in the feedback to the jack due to the very small displacement rate. The loading rate was 0.1 mm/min for the first two specimens (beams M45,D200,0.15 and M45,D200,0.3). It was then increased to 0.15mm/min for beams M30,D200,0.3, M45,D300,0.2 and M45,D300,0.3 and subsequently increased to 0.2mm/min for the rest of the specimens.

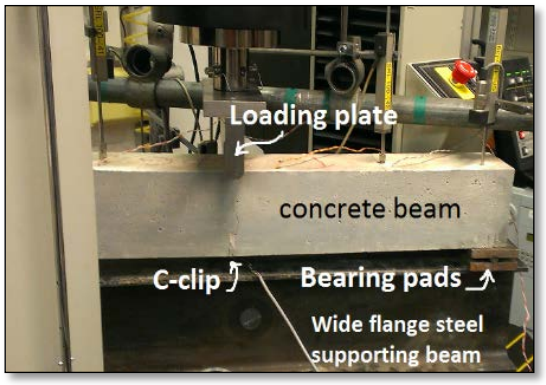

Figure 6 Photo of small beam test setup

Figure 7 Photo of large beam in test rig

4. Analysis and Results

A DIC analysis can result in subpixel accuracy through the usage of a subpixel interpolation scheme to interpolate between the discrete correlation coefficient values surrounding the maximum value. The accuracy is a function of the texture, bias error and gauge length in the case of strain measurements [43]. The measurement accuracy cannot easily be determined. However, there are various ways to improve the accuracy and to get an indication of the achievable accuracy range e.g. by increasing the contrast in the image colours. The bias error is dependent on the subpixel interpolation scheme and the accuracy with which the peak of the correlation coefficient can be determined [43]. Higher-order interpolation schemes can provide higher accuracy. GeoPIV software [44] was used in the current analysis. The software was developed at the University of Cambridge initially for geotechnical applications. GeoPIV has been shown by Lee et al. [43] to decrease the mean bias error to very small values (in the range between 0 - ±0.005 pixels) when a high-order subpixel interpolation scheme is implemented. In GeoPIV the correlation coefficient is calculated using a normalized cross correlation which enhances the accuracy of the matching process. The fracture evolution in the experimental specimens was tracked using the DIC. The results of DIC analysis depend on image length resolution, image search patch and distance between search patch centres [45]. The selection of these parameters depends on the problem under study where different image length resolutions, image search patches and distances between search patch centres need to be tested during the analysis [10,45]. In the current work the patch size was between 50 -100 pixels, the search patch size was between 200 – 300 pixels and the length resolution was 0.001 – 0.005 depending on the experiment set up, target area and the camera used. For more details, please refer to [46]. In the current study, the obtained values of the CMOD using DIC were verified against the C-clip gauge experimental results.

4.1. Experimental results

With the exception of beam M30,D100,0.5 all the beams failed in flexure when a central crack propagated in the region of the highest applied moment. Beam M45,D200,0.15 (Figure 8(a)), M30,D200,0.15 (Figure 8(b)), M45,D200,0.3 (Figure 8(c)), and beam M45,D100,0.3 (Figure 8(d)) exhibited a sudden failure due to reinforcement fracture. Beam M45,D300,0.3 (Figure 8(e)) exhibited a reinforcement fracture but with some rotation around the crack tip. However, Beam M30,D200,0.4 failed due to the failure of the bond between the reinforcement and concrete rather than reinforcement fracture (Figure 8(f)). Beam M30,D100,0.5 failed in shear and so will not be discussed further. Load-deflection curves of test beams are presented in Figures 9, 10, 11 and 12. Each figure compares a set of beams that have either the same size, similar concrete or the same reinforcement ratios. For the small beams the internal Instron machine readings were used to measure the deflections. For the medium and large beams the deflections were derived from the displacement of the loading jack. Corrections to account for any settlement of the testing system were made using the external LVDT readings at the beam supports.

There are drops in the load at some points along the curves because of the loading system and loading rate. The deflections at yield Δ_y for the medium and large beams were determined using the results of the strain gauges and are tabulated in Table 3. There were problems with the strain gauge readings in the small beams as they were located at the crack so they have not been included. It is of note that experimentally it was difficult to pinpoint the peak load due to the loading conditions so the maximum deflection was selected as the largest deflection associated with a load within ±5% of the peak load. This percentage was chosen because the average value of the peak load in the test beams was between 10-20 kN so that this percentage gives a load range of ±0.5-1kN around the peak load. With increasing reinforcement ratio, the maximum deflection at the peak load Δ_{max} increases (Table 3). The ductility factor based on the deflection ratio Δ_{max}/Δ_y was calculated (Table 3). From the tabulated results, it can be seen that the ductility appears to increase with increasing reinforcement ratio and beam size. It is worth noting that these trends only apply for lightly reinforced concrete beams that exhibit flexural failure. The beam behaviour is expected to become brittle with increasing reinforcement ratio and the onset of shear failures. The experimental results are in agreement with the findings in [28] for lightly reinforced concrete beams that were based on a numerical analysis and an energy-based definition of ductility. They are also consistent with theoretical predictions using an integrated fracture-based model for the analysis of lightly reinforced concrete beams [47].

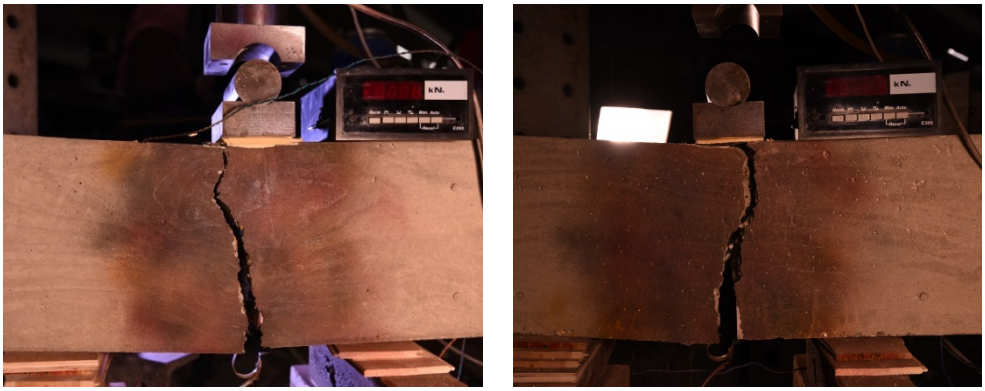

(a) (b)

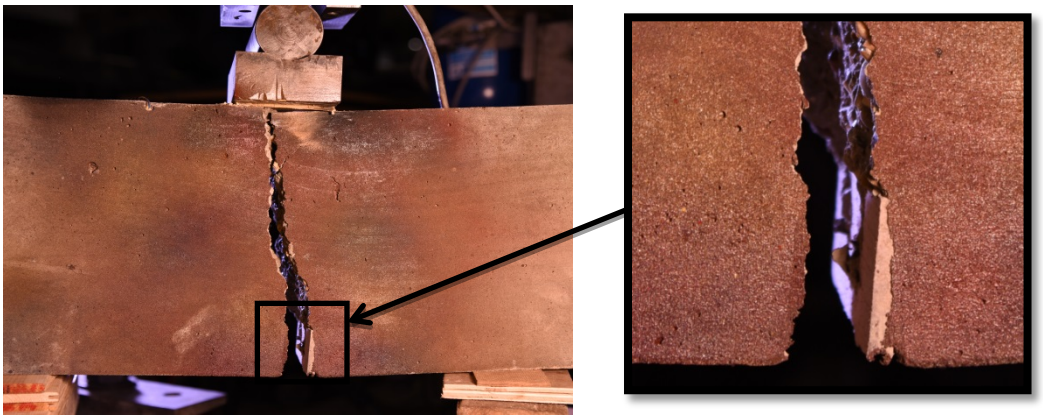

(c)

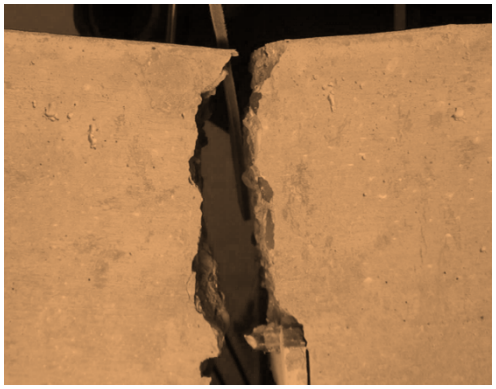

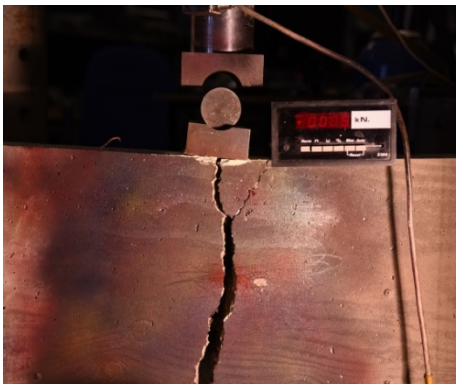

(d)

(e)

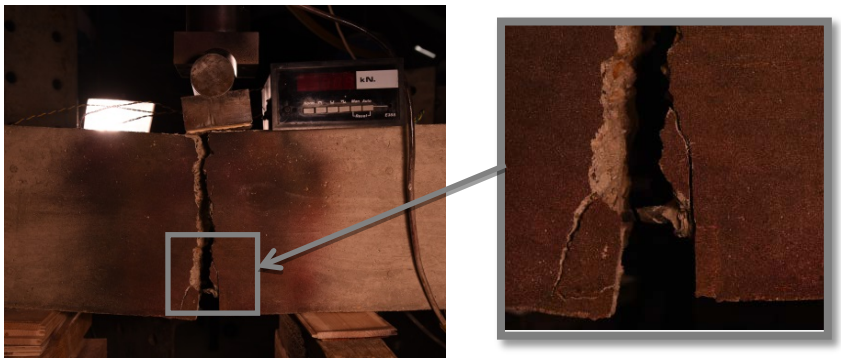

(f)

Figure 8 Failure modes of tested beams, (a) Beam M45,D200,0.15, (b) Beam M30,D200,0.15,(c) Beam M45,D200,0.3, (d) Beam M45,D100,0.5, (e) Beam M45,D300,0.3 and (f) Beam M30,D200,0.4

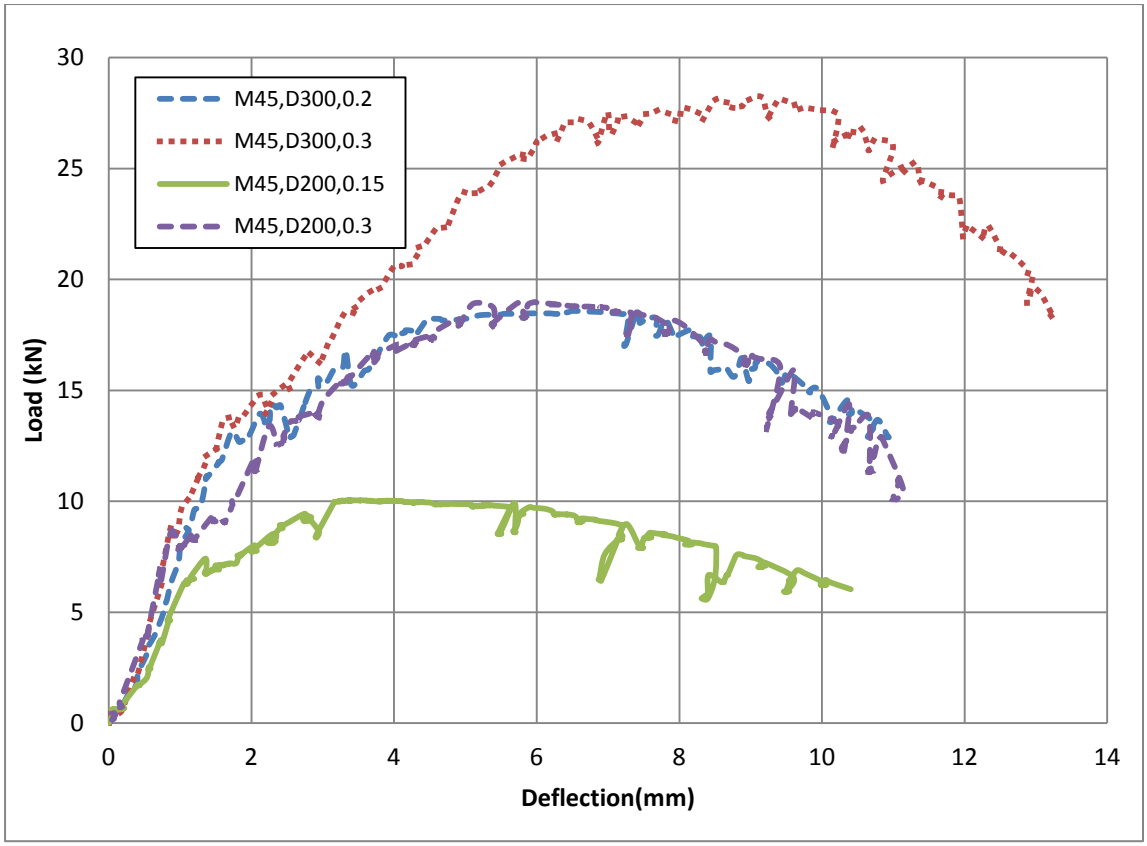

Figure 9 Load-deflection curves for beams M45,D300,0.2, M45,D300,0.3, M45,D200,0.15, and M45,D200,0.30

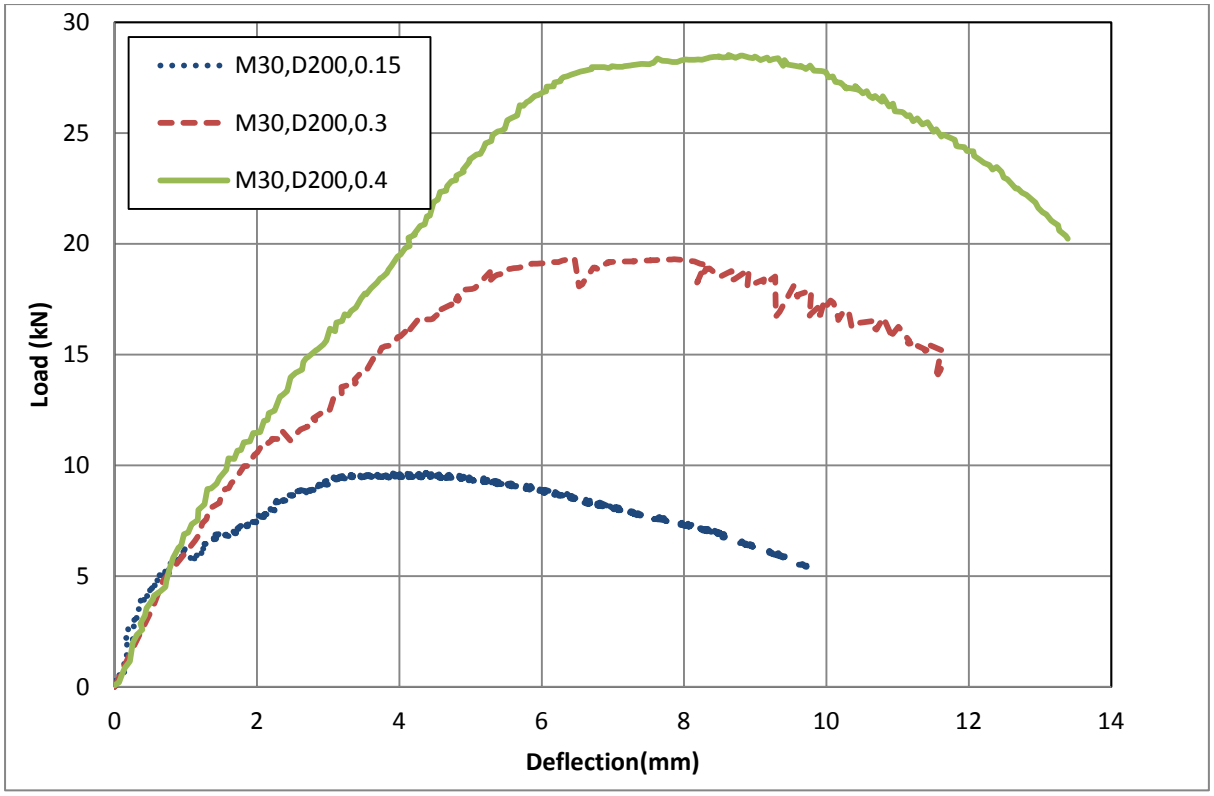

Figure 10 Load-deflection curves for beams M30,D200,0.15, M30,D200,0.3 and M30,D200,0.4

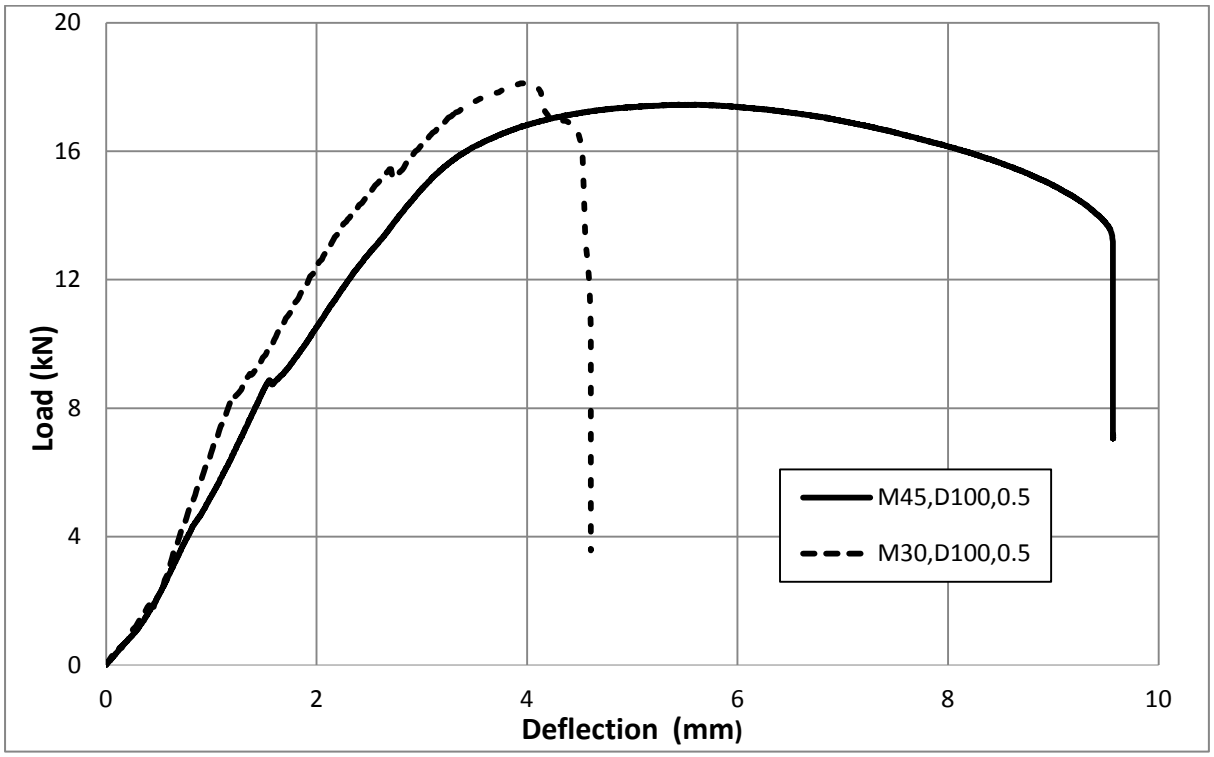

Figure 11 Load-deflection curves for beams M45,D100,0.5 and M30,D100,0.5

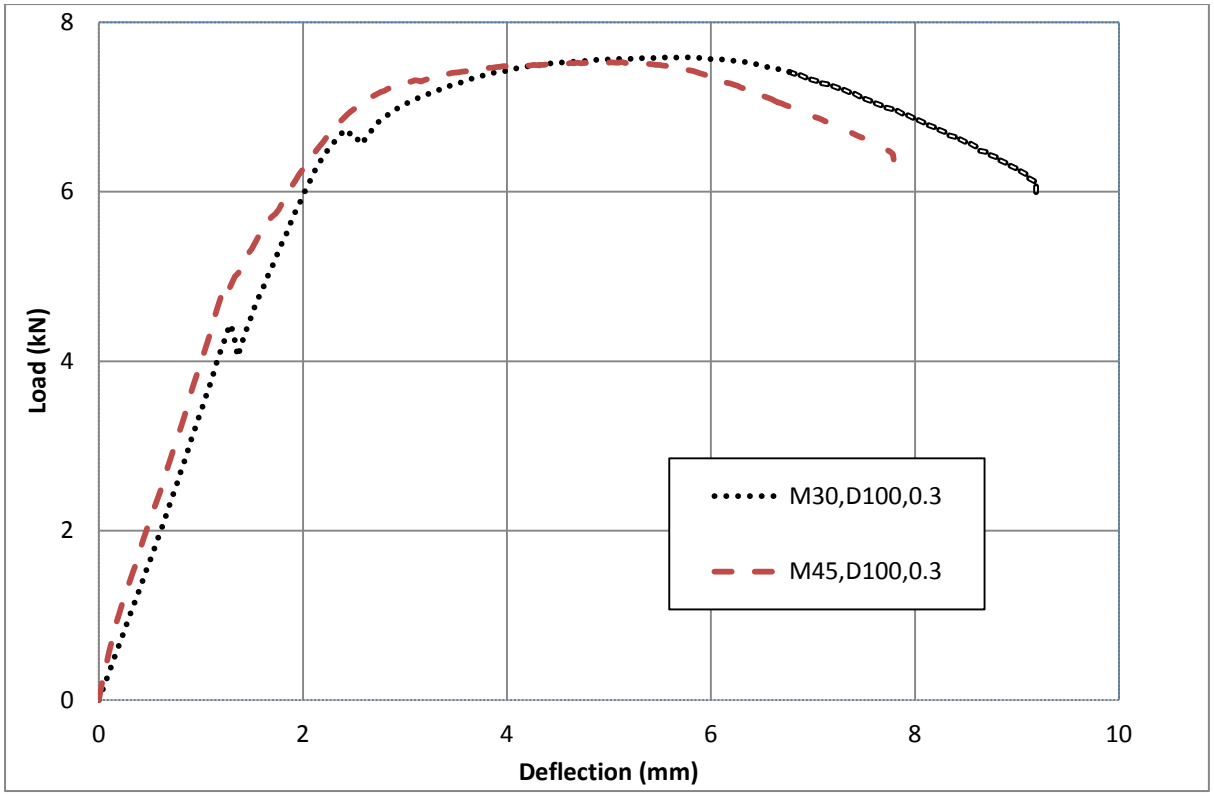

Figure 12 Load-deflection curves for beams M30,D100,0.3 and M45,D100,0.3

Table 3 Ductility factors of test beams

Beam	**Deflection at yielding Δ_y (mm)**	**Max. deflection at peak load ±5% Δ_{max} (mm)**	**$\mu = \Delta_{max}/\Delta_y$**
M45,D300,0.2	3.9	7.9	2.03
M45,D300,0.3	4.5	10.7	2.37
M45,D200,0.15	3.2	6.1	1.91
M45,D200,0.3	4.0	8.1	2.02
M30,D200,0.15	3.1	5.5	1.80
M30,D200,0.3	4.9	9.3	1.89
M30,D200,0.4	5.4	10.7	1.99

4.2. Fracture behaviour

The reinforcement bridges the crack and exerts a force that opposes crack opening. In this section, crack profile observations are presented to investigate the fracture evolution in reinforced concrete. One unreinforced beam was tested in each series to establish the baseline concrete fracture properties. This helps to understand the effect of the reinforcement on the fracture behaviour of concrete. The unreinforced specimens failed due to a crack propagating from above the crack tip. Figure 13 shows the load-deflection curve of a typical unreinforced specimen (M45,D200,0). During testing there was a delay in the control feedback to the jack and unfortunately the loading rate selected for this beam (0.1 mm/min) meant that steps in the load-deflection curve were noted. However, this was resolved for subsequent beams. Snapshots of the DIC strain profile until failure for M45,D200,0 are presented in Figure 14. It is of note the shape of the FPZ is a single curved band indicating the development of damage in the material. A softening behaviour follows the peak load where the load decreases with increasing vertical deflection. A considerable increase in the crack mouth opening occurs in the softening phase (Figure 15) and 90% of the total CMOD occurs in this stage. The final macro-crack propagation path coincides with the FPZ profile. Again these findings agree with existing literature [15–17]. Figures 16 and 17 show selected pre-peak and post-peak strain profiles for beams that have the same properties as M45,D200,0 but are reinforced. Beam M45,D200,0.15 has a reinforcement ratio of 0.15% and beam M45,D200,0.3 has a reinforcement ratio of 0.3%. In the current work, the region with strain localisation, micro-cracking and macro-cracking is referred to as the localised zone since it is difficult to isolate each of these phenomena. Localisation can be observed prior to reaching the peak load and this localisation is concentrated in a narrow crack band around the crack path. In the reinforced specimens this band starts as a single slightly curved zone but, with increasing load, the crack propagation continues along two branches. To identify the exact load at which branching occurs necessitates an image sequence with a high frame capture rate throughout the test and this was not possible in the current work. But even with more extensive images, the visual identification of the point of bifurcation, and the also width of the localised zone, would be somewhat subjective unless a standard definition of strain to indicate the transition from localisation to a macro-crack was clearly defined. This is the subject of further work. Nevertheless, for Beam M45,D200,0.15 the onset of branching seems to occur at some point between the images at 7.7kN and 9.25kN (Figure 16) whereas for M45,D200,0.3 it develops somewhere between 17.9kN and 18.3kN. Selected strain profiles for beams M45,D300,0.2 and M45,D300,0.3 during crack propagation and softening are displayed in Figure 18 and Figure 19 respectively. The localised zone advances in a single narrow band exhibiting some deviations from a straight line due to the heterogeneity of the concrete and aggregate interlock until it bifurcates into two branches. It can be seen that the branched localised zone was created in the two beams at a load of around 18kN in M45,D300,0.2 and 25kN in M45,D300,0.3 prior to the peak loads of 18.5kN and 28.2kN respectively. With increasing load, the branched localised zone develops and its length increases. The bifurcation took place in beam M45,D200,0.15 at a depth of 0.79 of the

effective beam depth and at a depth of 0.71 in beam M45,D300,0.3. In Figure 20, the beam depth is plotted against the relative depth at which bifurcation took place. In the larger beams branching occurs at a lower relative height than in the smaller beams. Also, the beams with a lower concrete strength typically showed a lower relative depth of branching although M45,D200,0.15 was the exception. After the onset of branching, localisation continues to develop at the tips of the two branches until one of the branches dominates and leads to final failure. The macro-crack propagation path therefore coincides with the localisation path. There is no clear trend in terms of the effect of the reinforcement ratio on the effective depth of branching in Figure 20. This is thought to be due to the different failure modes exhibited by the specimens. Beams M45,D300,0.2 and M45,D300,0.3 failed due to the sudden fracture of the longitudinal reinforcement and it was noted that the crack branching in beam M45,D300,0.3 started at a lower effective depth than that of beam M45,D300,0.2. A similar trend was observed in beams M30,D200,0.15 and M30,D200,0.3 where beam M30,D200,0.3 had a lower effective depth of branching than beam M30,D200,0.15. However, beam M30,D200,0.4 failed due to the failure of bond between the reinforcement and concrete at a higher relative depth than M30,D200,0.3. Beam M45,D100,0.5 also failed due to a bond failure whereas beam M45,D100,0.3 failed due to reinforcement fracture. Beams M45,D200,0.15 and M45,D200,0.3 failed due to the sudden fracture of the longitudinal reinforcement and beam M45,D200,0.3 had a higher effective depth of branching than that of beam M45,D200,0.15. This makes it difficult to make a clear conclusion about the effect of size on crack branching, and hence, on beam ductility. More specimens are required to be able to compare beams with similar failure modes. However, the reinforcement ratio does seem to have an effect on the branching angle. The different bifurcation angles for the beams are shown in Figure 21. It is of note that with increasing reinforcement ratio, the bifurcation angle seemed to become wider. For example, the bifurcation angles of beams M45,D300,0.2, M45,D200,0.15 and M30,D200,0.15 are relatively narrow when compared with the bifurcation angles of beams M45,D300,0.3, M45,D200,0.3, M30,D200,0.3 and M30,D200,0.4 which have higher reinforcement ratios. The dominant branch where the final failure occurred is highlighted in Figure 21. The load was applied to all the specimens in Figure 21 through the same width bearing pads. Stress concentrations at the edges of the loading pad may influence the crack branching and this could be explored further by undertaking studies where the width of the loading pad was varied. Crack branching generates a larger surface area that absorbs energy and hence more energy is needed for fracture to propagate. In the larger beams, branching occurred at a lower relative height than in the smaller beams. This means that for lightly reinforced beams, by increasing the beam size, a more ductile behaviour can be obtained. Crack branching occurred in all the reinforced beams but was not noted in the unreinforced concrete beams. Crack branching was previously reported in tests on small gravel unreinforced concrete beams [16] and it was suggested that further investigations on this phenomena were merited. In small unreinforced members this crack branching could be associated with a confinement effect due to aggregate interlock. In reinforced concrete, the reinforcement

provides an effective confinement to the crack path. The bifurcation occurs when the tip splits into two cracks. Where available, the strains in the steel bars when branching occurred are tabulated in Table 4. The strain values were in the range 0.0028-0.0033 and this means that the steel was yielding. Also, based on the results in Table 4 it can be seen that most of the CMOD in the tested beams happens after branching (or steel yielding as the two phenomena connected). 82% to 90% of the CMOD was noticed in the tested beams after crack branching. The strain profiles presented in Figures 16-19 suggest that crack branching occurred at loads of around 87-97% of the peak load, further indicating that the CMOD increases substantially close to the peak load. This indicates that before branching, the crack process is primarily about crack propagation whereas, after branching, crack opening dominates. The bifurcation leads to the failure in the compression zone in lightly RC beams. These observations are consistent with observations of the behaviour of concrete cylinders under compression [48] where it was concluded that an explanation for the mechanism of compressive failure requires consideration of cracking as well as bifurcation theory. Generally, a local bifurcation occurs when a parameter changes causing the stability of the equilibrium (or fixed point) to change. This may cause the emergence or disappearance of new stable points. There is a lack of a full and a clear explanation for the reasons for this phenomenon in reinforced concrete, not only in the current paper but also in RC studies. The aim of the current paper is to investigate experimentally this phenomenon and provide evidence that it is associated with the presence of reinforcement (or confinement effects). The results of the experimental program showed this within the range of the tested properties and within the tested sizes. The load deflection behaviour of the experimental reinforced concrete beams where bond failures did not occur (typically with a reinforcement ratio less than 0.3%) show a capacity for post-peak deflection which is reflected in the ductility factors presented in Table 3. As the crack bifurcation is associated with ductility, it is postulated that a better understanding of crack branching and the incorporation of the experimental observations into theoretical models would give a better prediction of the cracking process and a better estimation of the ductility. This could lead to an improved evaluation of the minimum flexural reinforcement required for ductile behaviour and will be the subject of further investigation.

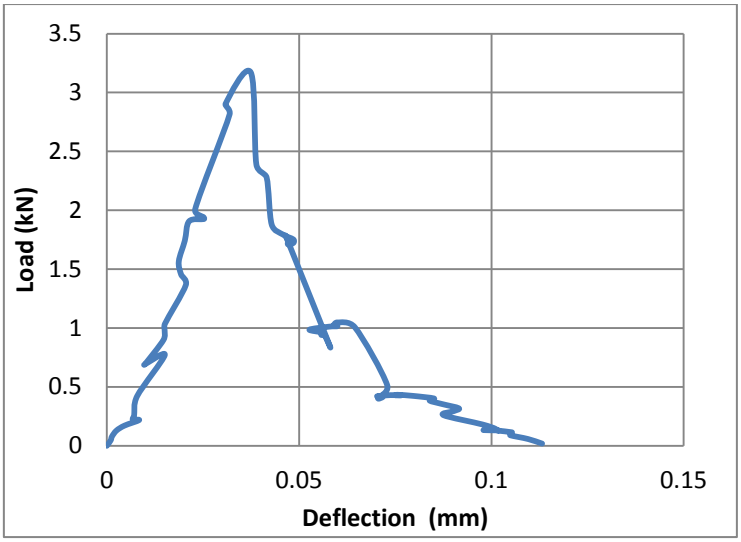

Figure 13 Load deflection behaviour of beam M45,D200,0

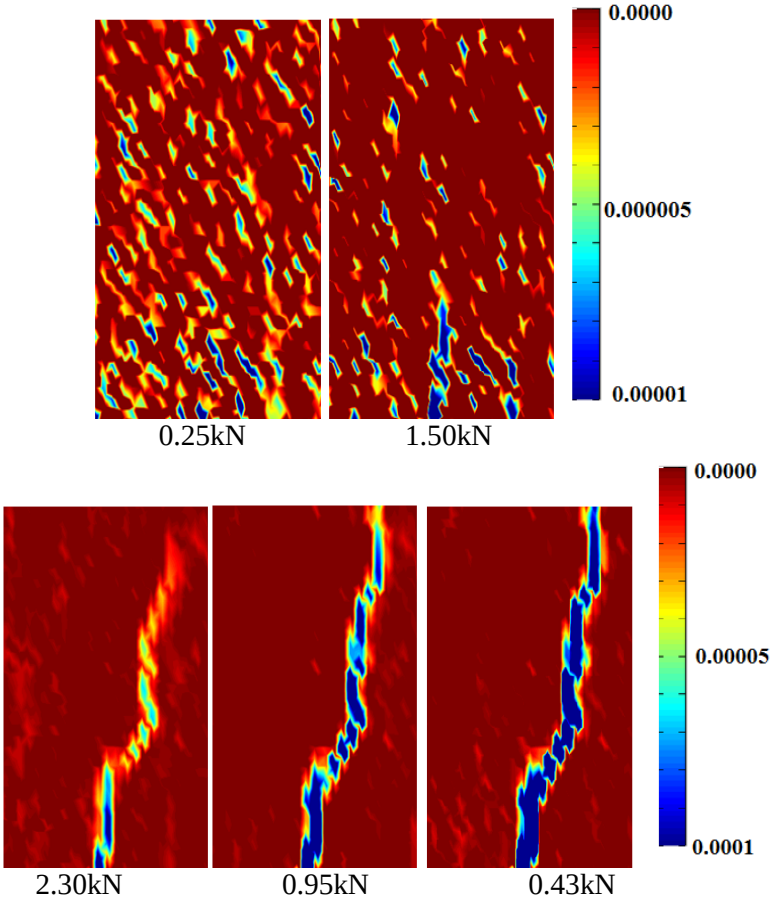

Figure 14 Strain profile in beam M45,D200,0

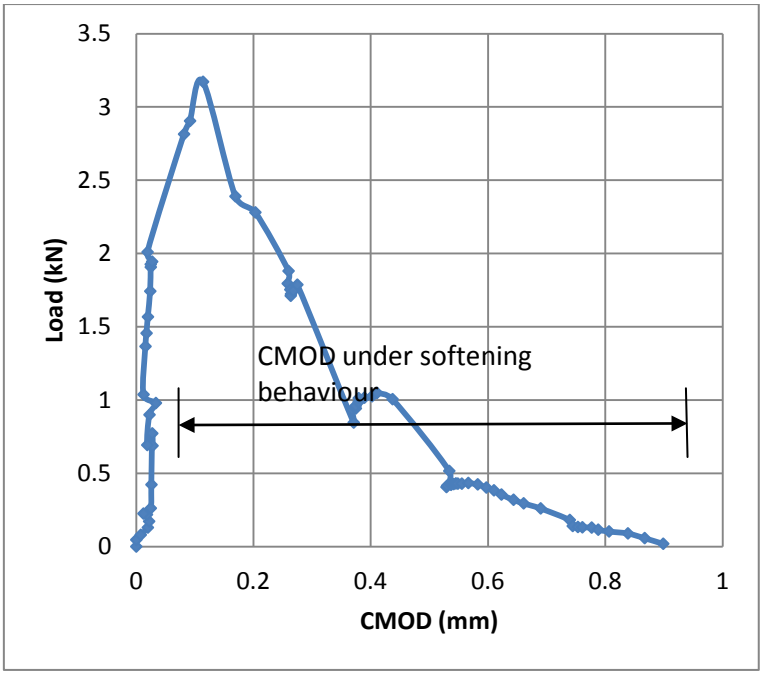

Figure 15 CMOD for beam M45,D200,0

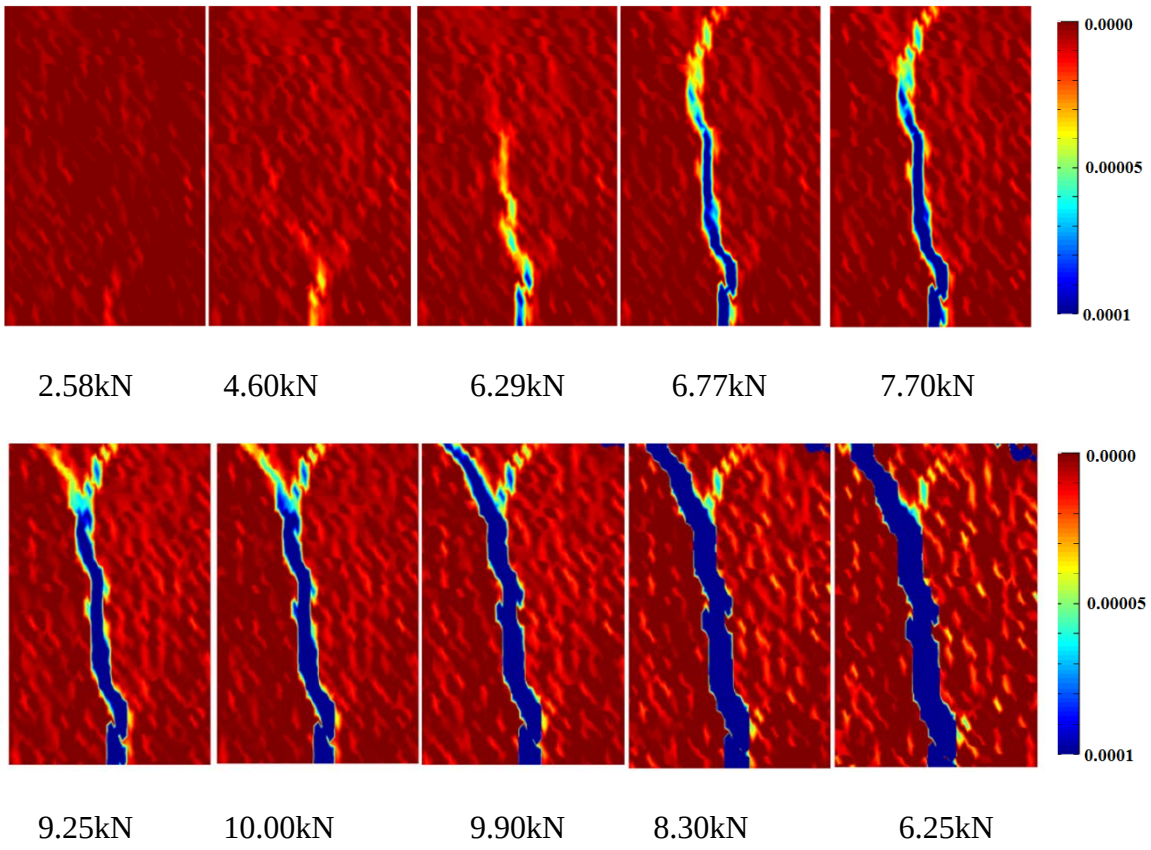

Figure 16 Strain profile in Beam M45,D200,0.15

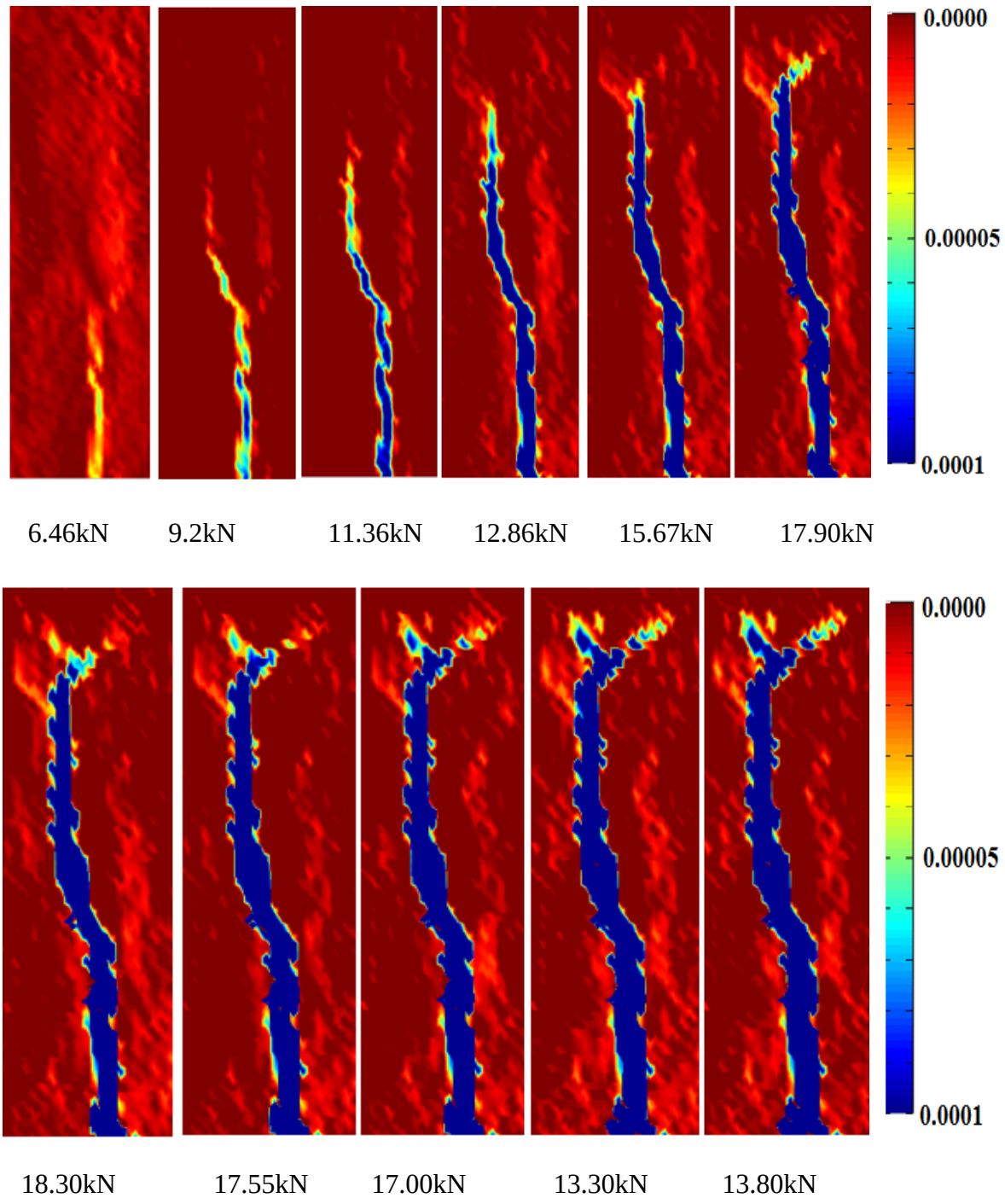

Figure 17 Strain profile in beam M45,D200,0.3

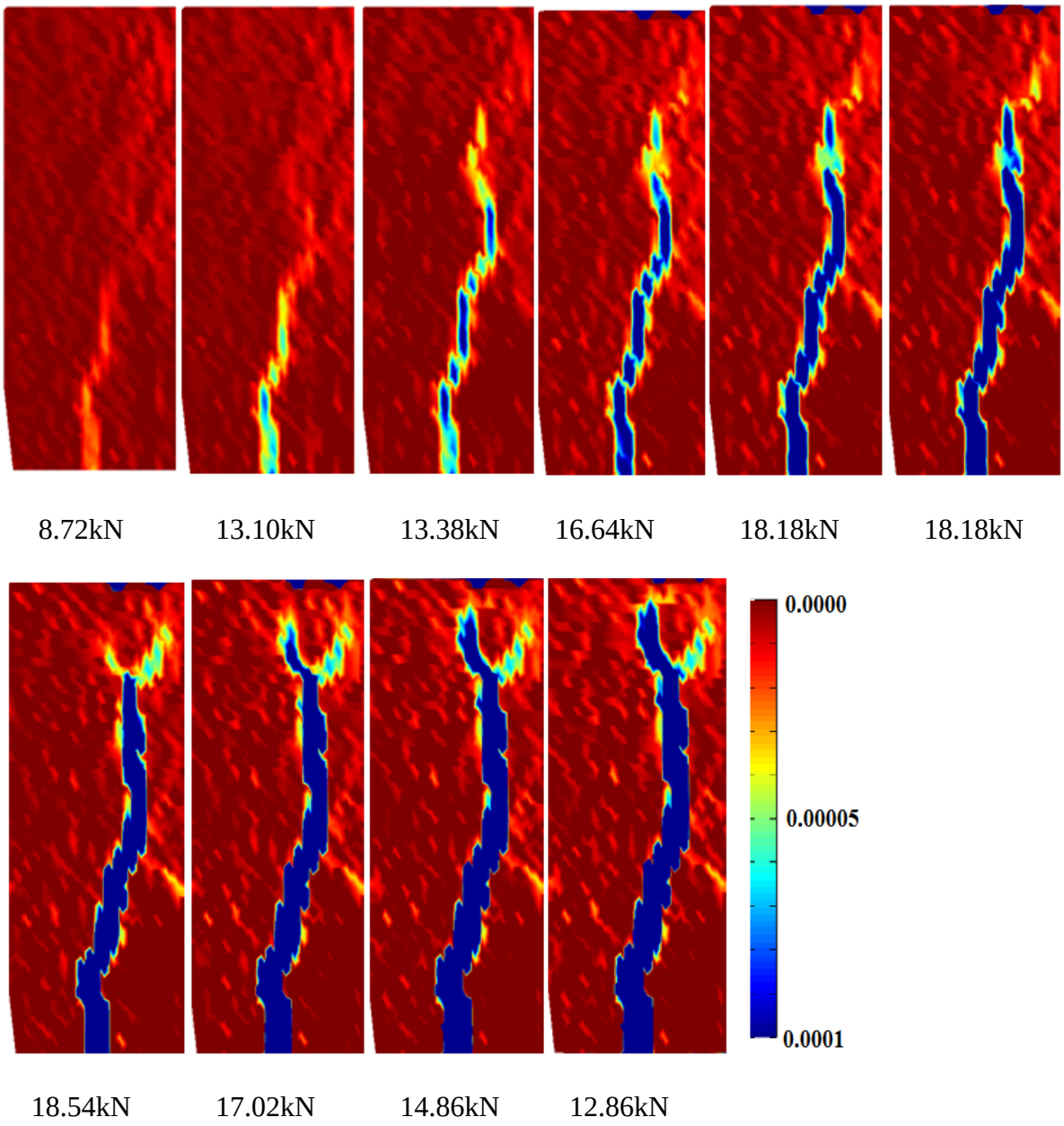

Figure 18 Strain profile in Beam M45,D300,0.2

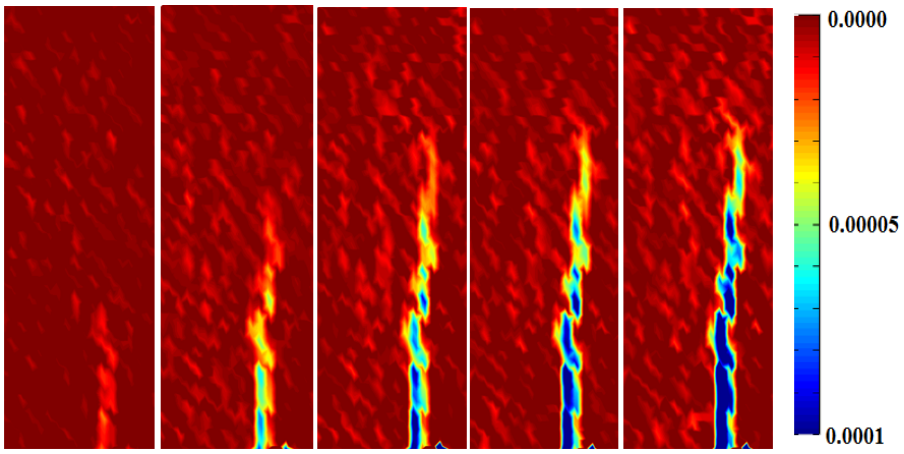

8.3kN 13.88kN 16.20kN 20.56kN 23.86kN

Zoomed in photos of the crack tip:

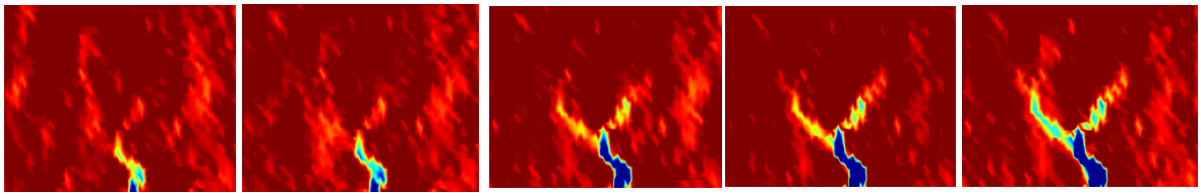

25.00kN 27.00kN 27.55kN 27.30kN 27.70kN

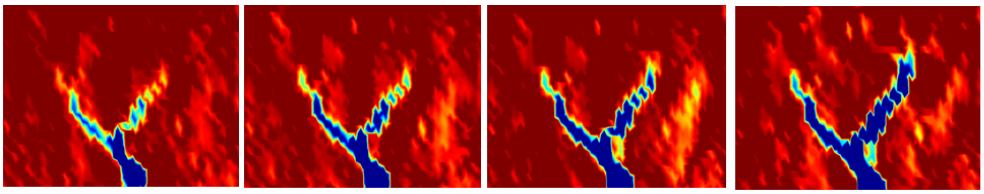

28.00kN 28.85kN 23.71kN 18.26kN

Figure 19 Strain profile in Beam M45,D300,0.3

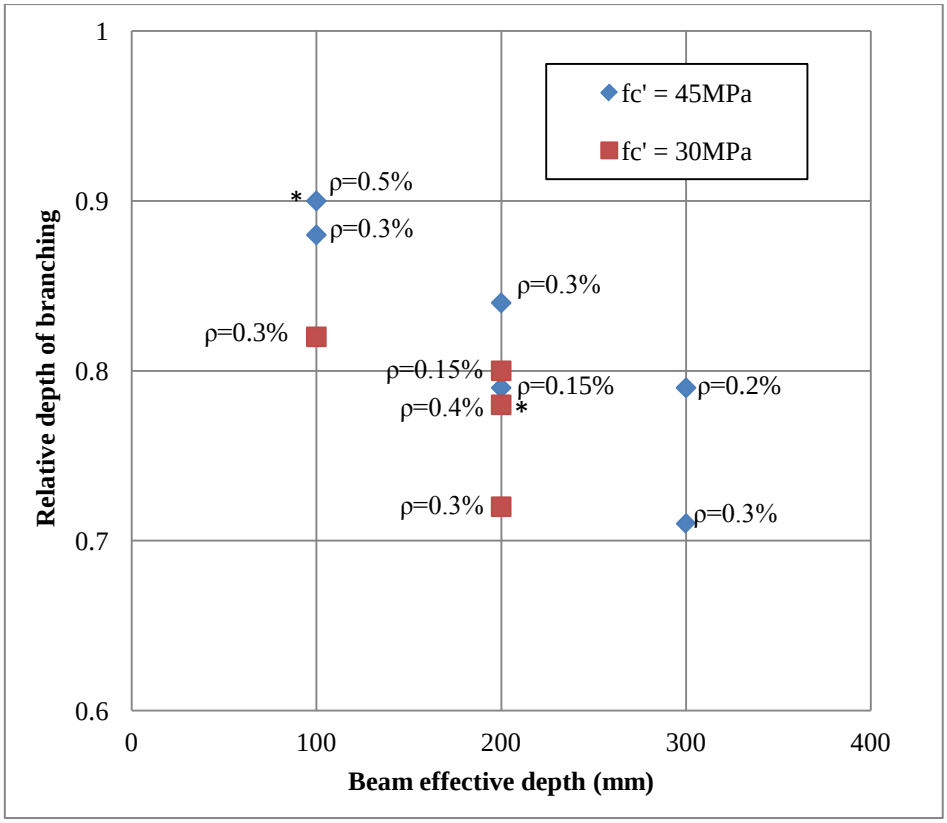

Figure 20 Beam effective depths versus the relative depths at which branching starts (denotes bond failure)*

Table 4 Measurements associated with crack branching

Beam	Steel strain at branching	CMOD at branching (mm)	Max. CMOD (mm)	% of CMOD that occurs after branching
M45,D300,0.2	0.0033	0.55	3.60	84.7%
M45,D300,0.3	0.003	0.42	4.07	89.6%
M45,D200,0.15	0.0029	0.67	5.20	87.1%
M45,D200,0.3	0.0028	0.8	4.45	82.0%
M30,D200,0.15	--	0.78	4.20	83.3%
M30,D200,0.3	0.0031	0.65	5.35	87.7%
M30,D200,0.4	0.0033	0.58	4.80	87.9%

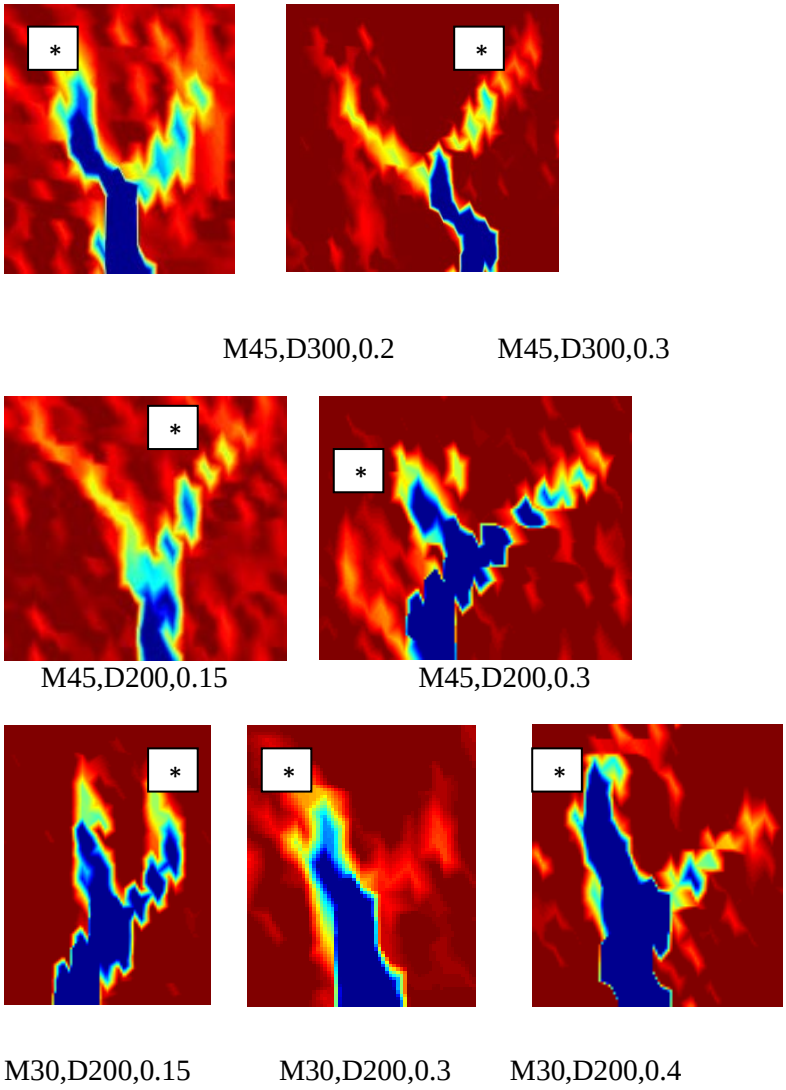

Figure 21 Bifurcation angles in different beams
(denotes the branch that dominated)*

5. Conclusion

An experimental investigation on the cracking process in RC beams was undertaken with a focus on the localised zone and crack branching phenomena. The following conclusions can be drawn based on the experimental results:

- The DIC technique enabled the visualization and quantification of the fracture properties in reinforced concrete. The DIC technique was found to be very effective in monitoring the crack propagation process when a high resolution camera was used.
- In unreinforced concrete beams the shape of the crack is in the form of a single curved band indicating the development of damage in the material. Softening behaviour ensues after the peak load where the load decreases with increasing vertical deflection. A considerable increase in the crack mouth opening occurs during the softening stage.

- In reinforced concrete, the crack initially propagates in the shape of a single narrow slightly curved band. However, the presence of the reinforcement prevents premature fracture and results in the development of crack branching where the single crack bifurcates. The combination of this bifurcation and cracking results in the failure of the compression zone. The final macro-crack propagation path coincides with the localization path.
- It has been shown that the larger the beam size, the lower the relative depth at which branching takes place. Also, beams with a lower concrete strength typically showed a lower relative depth of branching. The crack path is therefore influenced by both the magnitude and depth of the compressive stresses.
- In reinforced concrete, the bifurcation angle was fairly steep in beams with lower reinforcement ratios. With increasing reinforcement ratio, the bifurcation angle becomes shallower.
- Crack branching generates a larger surface area that absorbs energy. Hence more energy is needed for the crack to propagate and this affects the ductility of RC beams. It was found that increasing the beam size or the reinforcement ratio increases the ductility of RC beams according to a conventional definition of ductility.
- The experimental observations of the fracture process of RC beams need to be incorporated into analytical solutions for reinforced concrete cracking to develop better predictions for the cracking process of RC beams. This could lead to an improved estimation of the minimum reinforcement requirements for flexural members and associated ductility.

6. Acknowledgements

The authors would like to thank the Yousef Jameel Foundation and Cambridge Overseas Trust (COT) for their financial support of this research.

References

[1] Kaplan MF. Crack propagation and the fracture of concrete. ACI J Proc 1961;58:591–610.

[2] Hillerborg A, Modéer M, Petersson PE. Analysis of crack formation and crack growth in concrete by means of fracture mechanics and finite elements. Cem Concr Res 1976;6:773–81. doi:10.1016/0008-8846(76)90007-7.

[3] Bažant ZP, Oh BH. Crack band theory for fracture of concrete. Matériaux Constr 1983;16:155–77. doi:10.1007/BF02486267.

[4] Carpinteri A. Stability of fracturing process in RC beams. J Struct Eng 1984;110:544–58. doi:10.1061/(ASCE)0733-9445(1984)110:3(544).

[5] Jenq Y, Shah SP. Two parameter fracture model for concrete. J Eng Mech 1985;111:1227–41. doi:10.1061/(ASCE)0733-9399(1985)111:10(1227).

[6] Gerstle WH, Dey PP, Prasad NN V, Rahulkumar P, Xie M. Crack growth in flexural

members. A fracture mechanics approach. ACI Struct J 1992;89:617–25.

[7] Carpinteri A, Carmona JR, Ventura G. Propagation of flexural and shear cracks through reinforced concrete beams by the bridged crack model. Mag Concr Res 2007;59:743–56. doi:10.1680/macr.2007.59.10.743.

[8] Ooi ET, Yang ZJ. Modelling crack propagation in reinforced concrete using a hybrid finite element-scaled boundary finite element method. Eng Fract Mech 2011;78:252–73. doi:10.1016/j.engfracmech.2010.08.002.

[9] Mindess S. The fracture process zone in concrete. In: S. Shah, editor. Toughening Mech. quasi-brittle Mater., Dordrecht: Springer Netherlands; 1991, p. 271–86. doi:10.1007/978-94-011-3388-3.

[10] Skarżyński Ł, Syroka E, Tejchman J. Measurements and calculations of the width of the fracture process zones on the surface of notched concrete beams. Strain 2011;47:319–32. doi:10.1111/j.1475-1305.2008.00605.x.

[11] Wittmann FH, Hu. X. Fracture process zone in cementitious materials - Current trends in concrete fracture Research. Dordrecht: Springer Netherlands; 1991. doi:10.1007/978-94-011-3638-9.

[12] Wecharatana M, Shah SP. Predictions of nonlinear fracture process zone in concrete. J Eng Mech 1983;109:1231–46. doi:10.1061/(ASCE)0733-9399(1983)109:5(1231).

[13] Cedolin L, Dei Poli S, Iori I. Experimental determination of the fracture process zone in concrete. Cem Concr Res 1983;13:557–67. doi:10.1016/0008-8846(83)90015-7.

[14] Carpinteri A, Massabo R. Continuous vs discontinuous bridged-crack model for fiber-reinforced materials in flexure. Int J Solids Struct 1997;34:2321–38. doi:10.1016/S0020-7683(96)00129-1.

[15] Wu Z, Rong H, Zheng J, Xu F, Dong W. An experimental investigation on the FPZ properties in concrete using digital image correlation technique. Eng Fract Mech 2011;78:2978–90. doi:10.1016/j.engfracmech.2011.08.016.

[16] Skarżyński Ł, Tejchman J. Experimental investigations of fracture process using DIC in plain and reinforced concrete beams under bending. Strain 2013;49:521–43. doi:10.1111/str.12064.

[17] Alam S, Saliba J, Loukili A. Study of evolution of fracture process zone in concrete by simultaneous application of digital image correlation and acoustic emission. VIII Int Conf Fract Mech Concr Toledo, Spain 2013.

[18] Luchko II. Basic concepts of the fracture mechanics of reinforced concrete. Mater Sci 1996;31:448–53. doi:10.1007/BF00559138.

[19] Bosco C, Carpinteri A. Fracture behavior of beam cracked across reinforcement. Theor Appl Fract Mech 1992;17:61–8. doi:10.1016/0167-8442(92)90046-Z.

[20] Hillerborg A. Fracture mechanics concepts applied to moment capacity and rotational capacity of reinforced concrete beams. Eng Fract Mech 1990;35:233–40. doi:10.1016/0013-7944(90)90201-Q.

[21] Hosseini A, Mostofinejad D, Hajialilue-Bonab M. Displacement and strain field measurement in steel and RC beams using particle image velocimetry. J Eng Mech 2014;140:1–10. doi:10.1061/(ASCE)EM.1943-7889.0000805.

[22] Alam SY, Loukili A, Grondin F, Rozière E. Use of the digital image correlation and acoustic emission technique to study the effect of structural size on cracking of

reinforced concrete. Eng Fract Mech 2015;143:17–31. doi:10.1016/j.engfracmech.2015.06.038.

[23] Syroka-Korol E, Tejchman J. Experimental investigations of size effect in reinforced concrete beams failing by shear. Eng Struct 2014;58:63–78. doi:10.1016/j.engstruct.2013.10.012.

[24] Bažant ZP. Size effect in blunt fracture: concrete, rock, metal. J Eng Mech 1984;110:518–35.

[25] Beeteeo V. Ductility based structural design. Proc. Ninth World Conf. Earthq. Eng. Tokyo-Kyoto, Japan, Tokyo-Kyoto, Japan: 1988.

[26] Oudah F, El-Hacha R. Ductility of FRP reinforced RC structures: A critical review of definition and expressions. Concr. Solut. 2014 5th Intenational Conf. Concr. Repair, Belfast, Belfast: 2014.

[27] Park R. Evaluation of ductility of structures and structural assemblages from laboratory testing. Bull NZ Natl Soc Earthq Eng 1989;22:155–66.

[28] Carpinteri A, Cadamuro E, Corrado M. Minimum flexural reinforcement in rectangular and T-section concrete beams. Struct Concr 2014;15:361–72. doi:10.1002/suco.201300056.

[29] Vegt I, Breugel V, Weerheijm J. Failure mechanisms of concrete under impact loading. Fract. Mech. Concr. Concr. Struct. Fram., 2007, p. 579–87.

[30] Choi S, Shah SP. Measurement of deformations on concrete subjected to compression using image correlation. Exp Mech 1997;37:307–13. doi:10.1007/BF02317423.

[31] Wattrisse B, Chrysochoos A, Muracciole J-M, Némoz-Gaillard M. Analysis of strain localization during tensile tests by digital image correlation. Exp Mech 2001;41:29–39. doi:10.1007/BF02323101.

[32] Corr D, Accardi M, Graham-Brady L, Shah S. Digital image correlation analysis of interfacial debonding properties and fracture behavior in concrete. Eng Fract Mech 2007;74:109–21. doi:10.1016/j.engfracmech.2006.01.035.

[33] Fayyad TM, Lees JM. Application of digital image correlation to reinforced concrete fracture. Procedia Mater Sci 2014;3:1585–90. doi:10.1016/j.mspro.2014.06.256.

[34] Dutton M, Take WA, Hoult NA. Curvature monitoring of beams using digital image correlation. J Bridg Eng 2014;19:1–13.

[35] Jenq YS, Shah SP. Shear resistance of reinforced concrete beams- A fracture mechanics approach. ACI Spec Publ 1990;118:237–58.

[36] So KO, Karihaloo BL. Shear capacity of longitudinally reinforced beams-A fracture mechanics approach. Struct J 1993;90:591–600.

[37] Gastebled O, May I. Fracture mechanics model applied to shear failure of reinforced concrete beams without stirrups. ACI Struct J 2001;98:184–90.

[38] ACI318M-11. Building Code Requirements for Structural Concrete and Commentary. 2011.

[39] EC2:BS EN 1992. Design of Concrete structures. General Rules and Rules for Buildings. 2004.

[40] Pan B, Qian K, Xie H, Asundi A. Two-dimensional digital image correlation for in-plane displacement and strain measurement: a review. Meas Sci Technol 2009;20. doi:10.1088/0957-0233/20/6/062001.

[41] Schreier HW, Sutton MA. Systematic errors in digital image correlation due to undermatched subset shape functions. Exp Mech 2002;42:303–10. doi:10.1177/001448502321548391.

[42] Hoult N, Take A, Lee C, Dutton M. Experimental accuracy of two dimensional strain measurements using Digital Image Correlation. Eng Struct 2013;46:718–26. doi:10.1016/j.engstruct.2012.08.018.

[43] Lee C, Take WA, Hoult NA. Optimum accuracy of two-dimensional strain measurements using Digital Image Correlation. J Comput Civ Eng 2012;26:795–803. doi:10.1061/(ASCE)CP.1943-5487.0000182.

[44] White DJ, Take WA. GeoPIV: Particle Image Velocimetry (PIV) software for use in geotechnical testing. Cambridge: 2002.

[45] Skarżyński Ł, Kozicki J, Tejchman J. Application of DIC Technique to Concrete—Study on Objectivity of Measured Surface Displacements. Exp Mech 2013;53:1545–59. doi:10.1007/s11340-013-9781-y.

[46] Fayyad TM. Reinforced concrete crack analysis. PhD thesis, University of Cambridge, 2016.

[47] Fayyad TM, Lees JM. Integrated fracture-based model for the analysis of cracked reinforced concrete beams. Concr. 2015- 27th Bienn. Natl. Conf. Concr. Inst. Aust. Melb., Melbourne: 2015.

[48] Ikeda K, Yamakawa Y, Maruyama K, Emoto M. Bifurcation and fracture in reinforced-concrete specimens under compression. Third Int. Conf. Fract. Mech. Concr. Struct. -FraMcoS3, Freiburg, Ger., Freiburg, Germany: 1998.